The XMM-Newton View of GRS1915+105

Andrea Martocchia, Giorgio Matt, Tomaso Belloni, Marco Feroci, Vladimir Karas, Gabriele Ponti

Astronomy & Astrophysics manuscript no.
(will be inserted by hand later)

The XMM-*Newton* view of GRS 1915+105⋆

A. Martocchia[1⋆⋆], G. Matt[2], T. Belloni[3], M. Feroci[4], V. Karas[5], G. Ponti[6,7,8]

[1] CNRS / Observatoire Astronomique de Strasbourg, 11 Rue de l'Université, F–67000 Strasbourg, France
[2] Dipartimento di Fisica, Università degli Studi "Roma Tre", Via della Vasca Navale 84, I–00146 Roma, Italy
[3] INAF / Osservatorio Astronomico di Brera, via E. Bianchi 46, I–23807 Merate, Italy
[4] INAF / IASF, Area di Ricerca di Tor Vergata, Via Fosso del Cavaliere 100, I–00133 Roma, Italy
[5] Astronomical Institute, Academy of Sciences, Boční II, CZ–140 31 Prague, Czech Republic
[6] INAF / IASF, Sezione di Bologna, via Gobetti 101, I–40129 Bologna, Italy
[7] Dipartimento di Astronomia, Università di Bologna, via Ranzani 1, I–40127 Bologna, Italy
[8] Institute of Astronomy, Madingley Road, Cambridge CB3 0HA, United Kingdom

Received... Accepted...

Abstract. Two XMM-*Newton* observations of the black-hole binary GRS 1915+105 were triggered in 2004 (April 17 and 21), during a long "plateau" state of the source. We analyzed the data collected with EPIC-pn in timing and burst modes, respectively. Reflection Grating Spectrometers were used only on April 21st. The source 2–10 keV flux is ~ 0.6 (unabsorbed: $0.9 \div 1.1$) $\times 10^{-8}$ in cgs units. While the light curves show only small amplitude variations (a few percent) at timescales longer than a few seconds, a QPO is seen at about 0.6 Hz – as expected in χ variability modes of GRS 1915+105, when the phenomenological correlation with the source flux is taken into account – possibly with a harmonic signal at 1.2 Hz. The pn spectrum is well fitted without invoking thermal disk emission, on the basis of four main components: a primary one (either a simple power law or thermal Comptonization models), absorbed by cold matter with abundances different than those of standard ISM; reprocessing from an ionized disk; emission and absorption lines; and a soft X-ray excess at ~ 1 keV. However, the last is not confirmed by the RGS spectra, whose difference from the EPIC-pn ones lacks a fully satisfactory explanation. If real, the soft X-ray excess may be due to reflection from an optically thin, photoionized disk wind; in this case it may lead to a way to disentangle intrinsic from interstellar absorption.

Key words. Black hole physics – Accretion, accretion disks – X-rays: binaries – X-rays: individuals: GRS 1915+105

1. Introduction

The well-known black-hole (BH) binary GRS 1915+105 is sometimes classified as a *superluminal microquasar* because of the impressive radio jets whose matter seems to move with superluminal velocity due to a relativistic effect (Mirabel & Rodriguez, 1994; Rodriguez & Mirabel, 1999; Fender et al., 1999). For a recent review of this source, including a general discussion of its properties, see Fender & Belloni (2004).

Due to very large obscuration, the spectral type of GRS 1915+105's companion (a K-M III star) was discovered only recently, via infrared observations (Greiner et al., 2001). This yielded evidence that the system, initially discovered in the γ rays (Castro-Tirado et al. 1992), belongs to the class of low-mass X-ray binaries (LMXBs). On the basis of the commonly adopted value of the source's inclination (70°; but see Maccarone, 2002, for a discussion), Greiner et al. (2001b) used the same observations to determine the mass of the central compact object, which has been constrained to $M_c = 14 \pm 4 M_\odot$, i.e. well above the maximum neutron star mass limit. Thus GRS 1915+105 is believed to host a BH with a gravitational radius $r_g = \frac{GM}{c^2} \sim 21$ km, so it is classified as a BH binary.

Reig et al. (2003) note that, although the phenomenology of GRS 1915+105 has been usually[1] described in terms of three spectral states named A, B, and C (the latter being low/hard and jet-dominated), in fact several source properties always correspond to the canonical *intermediate* (sometimes called *very high*) *state* of galactic BH sources (see Homan & Belloni, 2005, and Belloni et al., 2005, for a definition). This is confirmed by Done et al. (2004), who also note that the source's unique limit-cycle variability appears when the source radiates at super-Eddington luminosities. Many of the GRS 1915+105 properties can be related to the binary's evolutionary state: the giant companion star and the long orbital period (33.4 days,

Send offprint requests to: A. Martocchia, andrea.martocchia@cesr.fr

⋆ Based on observations obtained with XMM-*Newton*, an ESA science mission with instruments and contributions directly funded by ESA Member States and NASA.

⋆⋆ *Present address:* UPS / Centre d'Etude Spatiale des Rayonnements, 9 Av. du Colonel Roche, F–31028 Toulouse, France

[1] Based on the hardness ratio and position in the color-color diagram.

by far the longest of any LMXB (Greiner et al., 2001) indicate that the Roche lobe overflow occurs in a very wide binary. The cause of all the unique long, as well as short-term, variability of GRS 1915+105 is then linked to the evolution of the huge disk structure, which can contain enough material to mantain nearly-Eddington accretion rates over timescales of several years.

A strong and broad iron Kα line was present in *Beppo*SAX (Martocchia et al. 2002, 2004) and *ASCA* GIS (Miller et al. 2004) spectra of GRS 1915+105. *Rossi*-XTE PCA data are generally well-fitted including a broad iron line component (e.g. Done et al. 2004), but the energy resolution of this instrument does not allow discriminating among different line models. The Fe Kα emission was also compatible with the spectral fits of *Chandra* data, taken during a low/hard state of the source, as reported by Lee et al. (2002).

An XMM-*Newton* ToO observation of GRS 1915+105, which would allow us to study the iron line profile with enhanced spectral resolution and sensitivity, was proposed in the second Announcement of Opportunity (AO2). The observation was intended to be triggered by the occurrence of a "plateau" state of the source (Foster et al. 1996), similar to the one observed during the *Beppo*SAX 1998 observation; this was also necessary in order to have the source in a less dramatic variability state and at a lower flux level to minimize technical problems due to instrumental pile-up and telemetry. For the latter reason we also planned to observe in timing mode.

The observation was triggered in April 2004, divided into two parts with $\sim$ 4 days separation one from the other. In this paper, while presenting the results, we offer an XMM-*Newton* view of GRS 1915+105 for the first time. First of all we describe (in Sect. 2) the observations and data extraction methods, and details of the state of the source based on its variability and general considerations. In Sect. 3 the best-fit spectral models and related physical parameters are given. Finally, in the conclusions, we summarize these XMM-*Newton* measurements and put our results in the context of the known source properties and open issues.

2. Observations and data reduction

To trigger the ToO observation, we set a condition on variability (*rms* single-dwell points of *Rossi*-XTE ASM to stay < 9% within one day) and a condition on flux (*Rossi*-XTE ASM daily rate below a threshold of 30 cts/s).[2] Both triggering conditions were met during the long "plateau", a lower-flux state also characterized by a more intense radio emission (Foster et al. 1996), which lasted several weeks during the Spring of 2004 (Fig. 1). The observation could be therefore started, in EPIC timing mode, on April 17, 2004 (hereafter: *OBS1*).

However, the source counts were enough to saturate the telemetry, even after switching off the MOS and RGS. Thus a second part of the observation was performed on April 21, 2004 (hereafter: *OBS2*), this time in (EPIC-pn) burst mode.

[2] ASM is the *All Sky Monitor* onboard *Rossi*-XTE. We used the public ASM "Weather Map" mask, accessible at: http://heasarc.gsfc.nasa.gov/xte_weather/.

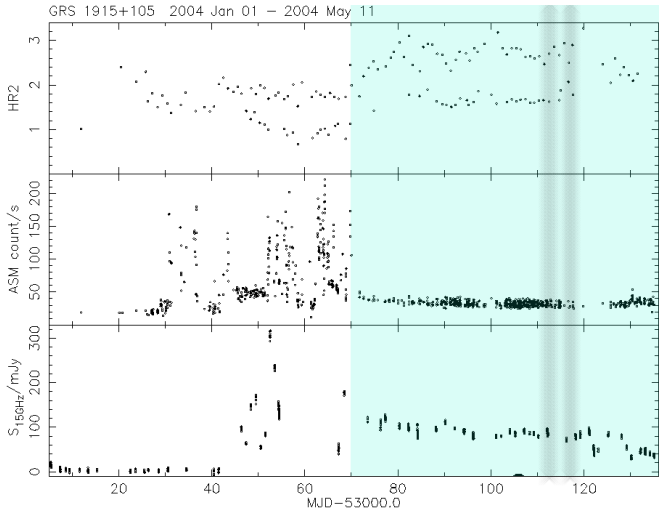

Fig. 1. Radio and X-ray light curves of GRS 1915+105 before and during the Spring 2004 plateau (starting at $\sim$ 2453070 JD), from: http://www.mrao.cam.ac.uk/~guy/. Radio data at 15 GHz were observed with the Ryle Telescope, Cambridge (see Pooley & Fender, 1997, for a description of the techniques used); X-ray data (ASM flux and hardness ratio) are taken from the *Rossi*-XTE quick-look web pages: http://xte.mit.edu/ASM_lc.html. The approximate dates of OBS1 and OBS2 are shaded. Note the anti-correlation between X and radio.

Given the typical plateau behavior, with strong jet activity and high radio level, we conclude that the source was caught in the conventional "hard" (C) spectral state and χ variability class, as defined by Belloni et al. (1997a,b, 2000), in both observations. This is similar to the condition in which the source was seen by simultaneous *INTEGRAL* (rev.57) and *Rossi*-XTE observations performed in the Spring of 2003 (Hannikainen et al. 2003, 2004, 2005; see Fuchs et al. 2003 for a multi-wavelength study of one of these observations).[3]

Count rate thresholds for pileup in timing modes are reported in the XMM User's Handbook.[4] The MOS count rate registered in both observations ($\sim$ 130 and 160 cts/s) is well above the quoted limit (100); therefore EPIC-MOS data are unusable,[5] and we restricted the analysis to EPIC-pn and RGS data (the latter are available only for OBS2).

Since in this state the source is stable, we can use the whole integration time to obtain very high statistics and signal/noise. Through adopting the customary method of extracting high-energy (E > 10 keV) background light curves, we checked for intervals of low contamination in both observations. While no background flaring is apparent during OBS1, we did initially select a 9 ks low-background interval (198951000 ÷ 198960000 s) in OBS2. We performed preliminary OBS2 data analysis

[3] This radio-loud state had been described already by Muno et al. 2001, and by Trudolyubov 2001 (as "type II").

[4] See Table 3 in: Ehle et al. (2004) – http://xmm.vilspa.esa.es/external/xmm_user_support/documentation/uhb/node28.html#2828

[5] Excising the core of the PSF is enough to cope with this problem in the case of imaging modes, but it is not applicable for timing modes.

with this selected dataset, then afterwards verified that the results were not modified when considering the whole observing interval. Therefore, in the following, we report results of the data analysis that was performed using *all* observing time, e.g. with the highest possible statistics. This also allowed us to refine the spectro-variability analysis (e.g. the analysis of root mean squared variability vs. energy: Ponti et al. 2004) as much as possible, which we performed to possibly disentangle the various contributions to the observed spectra and, thus, to get an independent validation of the adopted emission/absorption model. The high number of counts allows a high-resolution analysis of *rms* vs. E over the whole EPIC-pn energy band (about 35 energy bins for OBS2, and several dozen energy bins for OBS1; the minimum timescales of variation we could consider were, respectively, ~ 1000 and ~ 100 s). We used background-subtracted light curves in order to avoid contamination at the lowest and highest energies ($E \lesssim 2$ and $E \gtrsim 7$ keV), and found a mean *rms* value on the order of 5% ($0.02 \div 0.07$) in both observations, compatible with a null *rms* when Poisson noise is removed, with no visible features in the "*rms* spectra". We further verified this by studying $F_{\rm var}$ vs. E.[6]

The data were reduced with the standard SAS v6.1 and FTOOLS software packages. For EPIC-pn, single and double events were used in the timing modes (PATTERN <= 4); the fit was restricted to energies > 0.5 (> 0.4) keV in timing (burst) mode in order to avoid the increased noise. As recommended by the XMM-*Newton* Helpdesk, no selection on the RAWY coordinate was applied since this is related to a fine-time and the selection would therefore exclude certain time periods. However, RAWY < 160 was imposed as a condition in burst mode to avoid direct illumination by the source. Response and auxiliary matrices were created with the SAS tools rmfgen, arfgen, rgsrmfgen.

For the fit procedure we assumed a source distance of 12.5 kpc and inclination $i \sim 70^{\rm o}$ (Rodriguez & Mirabel, 1999; Fender et al., 1999).

2.1. First observation

The April 17 observation (OBS1: XMM-*Newton* rev.798, start time: 14:18:56 [JD2453113.096], stop time: 20:03:37 [JD2453113.336]) was performed in (both pn and MOS1) timing mode, as requested in the AO2 proposal mainly with the aim of avoiding pile-up problems. Moreover, the MOS2 camera and both RGS had to be switched off, to avoid overloading the telemetry. Nevertheless, the source flux was still so high that telemetry drops were frequent even in pn data, resulting in short gaps in the light curves, lasting a few to several seconds, for a total of about 75% of the observing time. They cause the search for (quasi-) periodic oscillations to be senseless on ~ 1 Hz timescales. Source light curves do not show any appreciable variations at timescales $\sim$ *a few* to ~ 100 s; however, as explained above (see Footnote 6), due to the full scientific buffer and telemetry drops, this result should be taken with caution.

Even though affected by telemetry drops for up to about 75% of the observing time, EPIC-pn data are well below the pile-up count rate threshold[7] and can therefore be safely used for spectral analysis.

The data were selected from a four-column strip centered on the source throughout the timing-mode (one-dimensional) "image"; a similar strip was selected far away from the source as a background sample.

2.2. Second observation

While the source essentially persisted in the same state, a second observation was started on April 21st (OBS2, rev. 800, start time: 13:49:23 [JD2453117.076], stop time: 20:56:55 [JD2453117.373]). To cope with the telemetry problem, this time we used EPIC-pn in burst mode, MOS in timing mode, and RGS in high count rate (HCR) mode. The other cameras were off.

In this observation, a background flare is apparent at the very beginning both in EPIC and RGS data; however, due to the very high S/N and shortness of the flare, it does not really affect the spectra. Source data were selected from a six-column strip (i.e. two columns more than in timing mode, in order to increase the statistics) throughout the burst-mode (one-dimensional) "image"; a similar strip was selected, far away from the source, as a background sample.

The EPIC-pn data are affected neither by telemetry drops nor by pile-up, in this observation, and can therefore be used for both spectral and timing analyses. However, as far as timing/variability studies are concerned, some caution is necessary since burst-mode data suffer from the intrinsic photon loss related to the 3% duty cycle (cp. Footnote 6). While the light curves only show tiny variations (up to a few percent, but compatible with zero: see Fig. 2) at all timescales bigger than a few seconds, a quasi periodic oscillation (QPO) at about 0.6 Hz, with a possibly harmonic signal at 1.2 Hz, is seen in the EPIC-pn data collected in burst mode (Fig. 3). This frequency is expected in χ variability modes of GRS 1915+105, when the phenomenological correlation with the source flux is taken into account (c.p. Fender & Belloni 2004). A forrest of narrow peaks at $\nu > 100$ Hz is apparent, due to spurious signals of instrumental origin.

2.2.1. The RGS data

Thanks to their excellent energy resolution, RGS cameras should be able to reveal subtle details in the 0.3–2.0 keV band. However, the source is so strongly absorbed below $1 \div 2$ keV that these data do not actually add much information. We used

[6] The nominal time resolution is 29 and 7 microseconds for EPIC-pn timing and burst modes, respectively. However, all results derived from the light curves must be taken with caution: in the first observation, even after removing all telemetry drops, the collected photons "saturated" the instrument's bandwidth; therefore, energy-dependent oscillations in the count rate may have been "cut off". On the other hand, photons collected in the second observation, i.e. in burst mode, are selected on the basis of an *ad hoc* duty cycle in the reading process (events are not registered for 97% of the time).

[7] For EPIC-pn timing mode the pile-up threshold for a point source is 1500 cts/s, the telemetry threshold is 300 cts/s, while we registered ~ 650 cts/s.

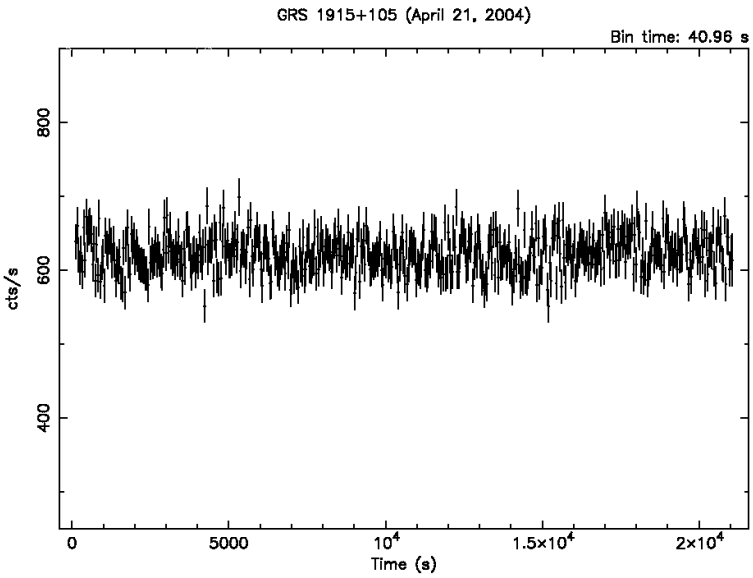

Fig. 2. The source light curve in the 0.4 – 10.0 keV band during OBS2 (EPIC-pn, burst mode, *not* background-subtracted). The whole 20946 s observation has a mean 618 (i.e. 18.54/0.03) cts/s; the background has just about 18 (i.e. 0.5320/0.03) cts/s.

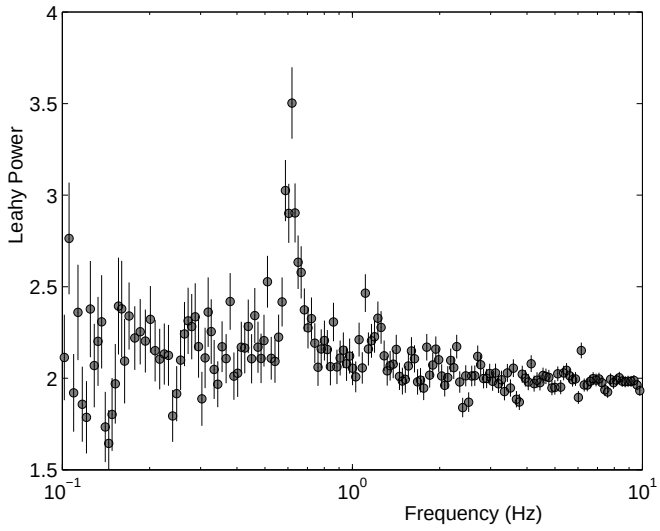

Fig. 3. Power spectrum in the 0.4 – 13.0 keV band of the OBS2 (April 21) EPIC-pn data.

them mainly to check the EPIC-pn spectrum: in Fig. 4 we show the 0.5-2 keV spectra of both instruments, fitted with a simple absorbed power law model, with Γ fixed to 2 (see Sect. 3.2).[8] The RGS and EPIC-pn spectra are clearly different, especially with regard to the broad excess around 1 keV in the

[8] Multiplicative constants to the RGS have also been added to allow for intercalibration problems (the best fit values for the constants are 1.28 and 1.22 for the RGS1 and RGS2, respectively). RGS data, collected in the standard CCD read-out scheme, are marginally affected by pile-up, which amounts to a few percent and mainly affects the energies where the spectrum peaks.

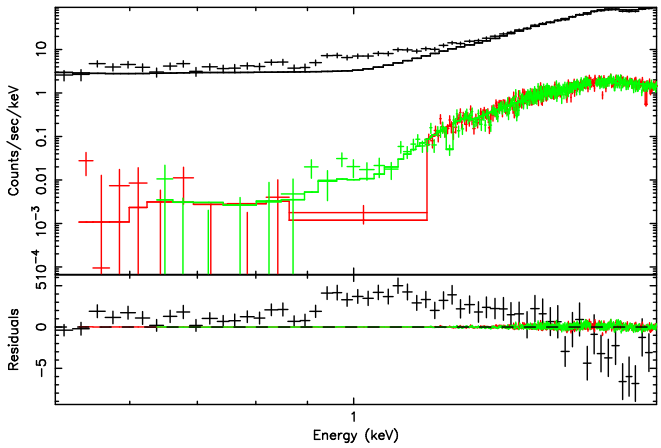

Fig. 4. The RGS and pn (burst mode) spectra fitted in the 0.5-2 keV range with a simple absorbed power law. The RGS and pn spectra clearly disagree each other.

latter spectrum. The RGS spectrum shows a fast decline (more than two orders of magnitude, with very few counts at the lower energies), without any apparent features. In Sect. 3.1.5 we go through the alternative hypotheses that can be invoked to explain the RGS–pn discrepancy.

RGS normally have a 15 ms timing resolution in HTR mode; we produced standard light curves, but did not get any useful results due to the low statistics on most of the band.

3. Spectral analysis

At the flux level of GRS 1915+105 ($\sim 10^{-8}$ erg cm^{-2} s^{-1}), it is very likely that systematic errors cannot always be neglected with respect to the statistical ones. However, introducing an energy-independent systematic uncertainty would prevent a meaningful use of the χ^2 statistics. Features at the 1-2% level must therefore be taken with caution as possibly of instrumental origin (cp. Kirsch 2005).

Even though the background issue is not relevant on most of the energy band, due to the extremely high S/N, nevertheless it may play a role at the highest energies ($E \gtrsim 10$ keV), as well as at the energies where the source is strongly absorbed ($E \lesssim 1.5$ keV). We therefore performed background subtraction; all reported results refer to background-subtracted analysis, unless stated otherwise. Of course, if a dust halo is present (cannot be checked with our data, given the lack of imaging capabilities of the timing modes; but see Greiner et al., 1998, on the issue), background subtraction may cause a spectral distortion in the soft band, depending on the distance from the source at which the background spectrum is taken (see below, Sect. 3.1.5).

Spectra were rebinned in order to have about three bins per energy resolution element and at least 20 counts per bin at the same time. Spectral fits were performed with the XSPEC v.11.3.0 software package. In the following, all errors refer to a 90% confidence level for one interesting parameter ($\Delta\chi^2$=2.71).

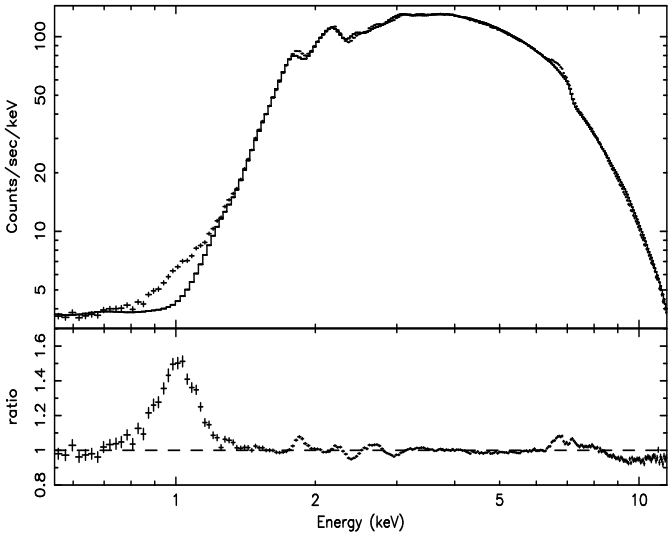

Fig. 5. The OBS1 spectrum and data/model ratio when fitted with a simple power law and cold absorption with variable abundances.

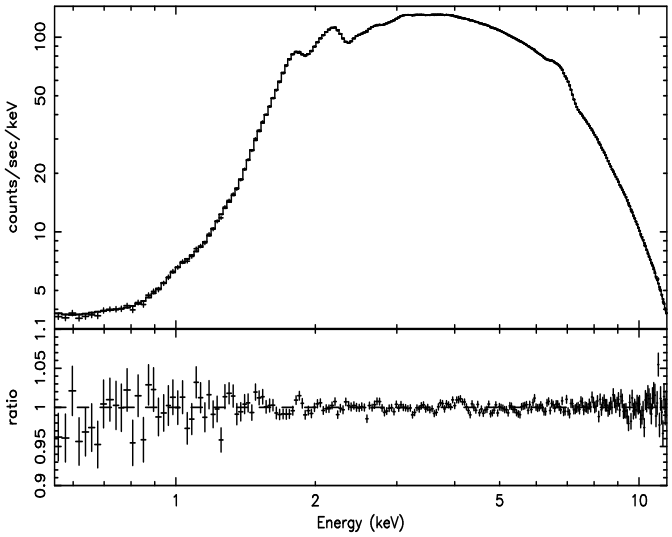

Fig. 6. The OBS1 spectrum and data/model ratio for the best fit model (see text and Table 1).

3.1. The timing-mode observation

As discussed in the previous section, we are confident that the telemetry problems do not affect the spectrum significantly. Given the much larger total number of counts in OBS1, we decided to use it first for the spectral analysis.

To illustrate the spectral complexity, in Fig. 5 we show the best fit spectrum and data/model ratio after fitting with a simple power law absorbed by cold matter. Element abundances were left free to vary with respect to the solar value ratios. Several features are apparent: an excess around 1 keV, several wiggles between $\sim$ 1.5 and 3 keV, an excess at the energies of the iron line complex, and a deficit above 8 keV.

After several attempts, we found a – both statistically (χ^2/d.o.f.=317.5/227) and physically – reasonable description of the spectrum in terms of (see Table 1, and Fig. 6) a power law with $\Gamma \sim$1.7, several absorption and emission features, an ionized and optically thick reflection component (and/or a warm absorber), and an optically thin reflection component to model the 1 keV excess. Given the fact that all remaining deviations of the data from the model are no larger than about 1-2%, i.e. on the order of the systematic errors in the calibration (which, for most of the energy range under analysis, is larger than the statistical errors), we did not try to improve the fit further.

We now discuss the various spectral components separately for the sake of clarity.

3.1.1. The continuum

First of all, we note that a simple power law is basically sufficient to describe the continuum, apart from an additional component required to fit the >8 keV deficit and an apparent broad excess around $\sim$ 1 keV. Substituting the power law with simple Comptonization models (like or) does not lead to any significant improvement in the fit. No thermal emission from an accretion disk is apparent (the inclusion of a multicolor disk component is not required by the data). Of course, this strongly suggests that the innermost disk regions were absent during the observation. The apparent 1 keV excess is far too narrow to be fitted by even a single temperature blackbody (i.e. the narrower among physically motivated continuum models) or to be residual from "distorted" disk thermal emission. The nature of this feature will be discussed separately in Sect. 3.1.5.

3.1.2. The cold absorber

The photoelectric absorption has been fitted with the XSPEC model , which assumes neutral matter and allows the elemental abundancies to vary separately. In practice, for the sake of simplicity, we grouped the elements so that within each group the elements are linked as: H, He, C, N, O; Ne, Na; Mg, Al; Si; S; Cl, Ar, Ca, Cr; Fe, Co, Ni. The rationale behind this choice is both physical and practical. In fact, we grouped elements together whose origin is very likely common, but also those which are less abundant (and therefore cannot be measured easily independently) with very abundant ones: e.g. Co and Ni with Fe. We also grouped H and He with C, N, and O because their effect is small in our energy range.

In Table 1 the best fit values are reported. They are given in units of hydrogen equivalent column densities for solar abundances as in Anders & Grevesse (1989). A significant overabundance of the heavier elements with respect to the lighter ones is apparent. These results are only partly consistent with those derived from the *Chandra* HETG observation (Lee et al. 2002). In particular, Fe and S abundances are roughly the same, while our values for Mg are about twice, and 2/3 for Si. Fixing the abundances to the values of Lee et al. (2002), the fit is unacceptable (χ^2/d.o.f.=659.9/231). We note that our observation has a lower energy resolution, but many more photons.

These overabundancies with respect to the solar values (the differences are even greater assuming the ISM values, see Wilms et al. 2000) suggest that a significant fraction of the absorber is local to the source. The value for the low Z elements

(i.e. 1.6×10^{22} cm^{-2}) can then be assumed as the upper limit to the ISM absorber column density. It is interesting to note that this value is similar to the one estimated by fitting the ∼1 keV excess (see below).

3.1.3. Reflection or warm absorption?

The deficit above 8 keV can be fitted equally well by a simple smeared edge model ( ) or by an ionized and relativistically blurred reflection component ( ). As the smearing edge is not physically meaningful *per se*, but is usually assumed to represent the reflection component, we will not discuss the fits with this component further.

The model adopted for the disk reflection component includes the relativistic effects in Schwarzschild metric. The inner and outer radii are linked to those of the H–like iron line (see below). The disk inclination angle has been fixed to 70°, and the matter temperature to 10^6 K. The very large value of the inner radius (about $320r_g$) justifies *a posteriori* the use of the Schwarzschild metric instead of the Kerr one (differences between the two metrics, even for a maximally rotating BH, are insignificant above $\sim10r_g$), and it agrees with the lack of any detectable thermal disk emission. The iron abundance is five times the solar value, roughly consistent with the overabundance found in the cold absorber (see above). The ionization parameter is pretty large, in agreement with the presence of He– and H–like iron lines. The significant solid angle subtended by the disk to the illuminating source, i.e. $0.3\times2\pi$, implies that the emission occurs at distances comparable to the inner disk radius. The adopted model is necessarily a simplification of the real situation, as it adapts a unique ionization for the whole disk, while the ionization very likely decreases with increasing radius. The derived parameters, therefore, must be taken with caution and considered only as indicative.

The presence of a H–like iron absorption line (see below) suggests warm absorption. Substituting the reflection component with a warm absorber (model), a significantly worse, but not completely unacceptable fit is found (χ^2/d.o.f.=384.5/226), with a comparable iron overabundance ($A_{\rm Fe}$=6.6) and power law photon index ($\Gamma\sim1.69$). However, the column density ($\sim7.7\times10^{21}$ cm^{-2}) is larger than that implied by the value of the EW of the absorption line (see Table 1), given the large iron overabundance (e.g. Bianchi et al. 2005). Moreover, the presence of ionized disk lines (see below) *requires* the presence of the ionized reflection component. We thus fitted the spectrum with both the reflection and the warm absorber. No significant improvement is found with respect to the fit with the reflection only, but the upper limit to the column density, $\sim2\times10^{21}$ cm^{-2}, is now consistent with the absorption line EW.

3.1.4. The iron lines

In Fig. 5, a clear broad excess at the energy of the iron line complex is apparent. The excess is at larger energies than 6.4 keV, strongly suggesting ionized iron. We fitted this excess with two unresolved emission lines (σ=10 eV) peaking at 6.7 keV and 6.96 keV, which correspond to He– and H–like iron, respectively; and after Lee et al. (2002) we also included an unresolved absorption line with energy free to vary around the value of the H–like iron. The fit is unacceptable (χ^2/d.o.f.=617.2/225), and not surprisingly, the absorption line was not found. A much better, but still hardly acceptable, fit (χ^2/d.o.f.=425.6/223) is found when leaving the widths of the lines free to vary. We found σ=129 eV and 174 eV for the He– and H–like lines, respectively; an absorption line centered at ∼ 6.95 keV is also found. The high values of σ, along with the likely presence of the disk reflection component, strongly suggest that the lines are relativistically broadened: we therefore substituted the broad Gaussians with models, with the outer radius linked to that of the reflection component, as well as the inner radius of the H–like line (the inner radius of the He–like left free to vary, in the assumption that the matter is more ionized in the innermost regions). The results are reported in Table 1. The fit is significantly better than with the Gaussians and – as expected on both physical grounds and from the fact that the width of the He–like line is smaller – the inner radius for this line is larger than that of the H–like line (the values of the radius must of course be taken merely as indicative, see discussion above). The energy of the narrow absorption line, $6.95^{+0.01}_{-0.03}$ keV, is just below the rest frame value.[9] The line was assumed to be narrow ($\sigma\equiv1$ eV); when leaving σ free to vary, no improvement in the fit is found.

We also tried to fit the iron emission with just one disk line model, with the energy free to vary. The fit is of comparable statistical quality, but the line energy, 6.86±0.01 keV, does not correspond to any rest frame atomic energy of significance. Moreover, the good fit is obtained at the expense of a very large value for the iron abundance of the reflection component (∼18 times the solar value). Therefore, the model with two disk lines has to be preferred.

The EW of both lines (28 eV) seems rather small when compared to the amount of the reflection component (Matt et al. 1996). However, one must note again that the ionization most likely changes along the radius in the disk. While reflection occurs (even if with changing spectra) throughout the disk, line emission occurs only if the corresponding ion is present, which probably only happens in a fraction of the disk.

3.1.5. The ∼1 keV excess

In Sect. 2.2.1 we have shown that, during the burst-mode observation, the RGS and pn disagree, with the former not showing the 1 keV excess. (Unfortunately, during the timing-mode observation the RGS were switched off). There are several possible explanations for both the excess and the RGS-pn discrepancy. As we will see, none of them is fully satisfactory, and we consider the issue still open as we wait for improvements in calibrations.

A pn instrumental origin for the broad excess seems unlikely for various reasons. The amplitude (about 40% of the underlying continuum, see the data vs. model ratio in Fig. 5) is far

[9] Actually, this is a blend of two lines, with centroid energy at 6.966 keV.

too large, given the known calibration uncertainties (cp. Kirsch 2005). Moreover, the excess is present in the Timing as well as in the burst mode, and was also observed with *Beppo*SAX (cp. Fig. 3 in: Feroci et al. 1998). A similar feature has also been seen in other binaries (see e.g. the case of the dipping LMXB 4U 1323-62: Boirin et al. 2005), but not in all; in particular, it is not present in the burst mode observation of the Crab Nebula (Kirsch et al. 2005).

However, given the unusual brightness of our source and the fact that the excess arises in the part of the spectrum where the count rate drops precipitously due to absorption, a calibration problem that is possibly related to the redistribution matrix cannot be completely excluded at the moment.

Let us then assume that this excess is real. We could not fit this feature with any continuum model put behind the whole absorber. As seen in Sect. 3.1.1, it cannot be fitted with blackbody models; the only model able to fit it is a broad Gaussian with an EW of several tens of keV, which has no physical explanation. Good fits are instead found if the emission is screened by a thinner absorber. There are three possibilities in this respect: (i) a confusing source, (ii) a dust scattering halo, or (iii) a component related to the system but lying outside the intrinsic absorber.

The confusing source hypothesis seems unlikely. In timing modes, source data are extracted from a narrow strip (here about 16"); the required, "polluting" source would have to be bright (0.5-2 keV observed flux of about 4×10^{-12} erg cm^{-2} s^{-1}): but no source is present in the *ROSAT* All Sky Survey within a radius of 0.3° around GRS 1915+105 (we checked with the HEASARC tool PIMMS that such a source would be well above the typical RASS detection limit; of course, the possibility of a variable source cannot be ruled out).

Since the dust scattering is energy dependent, ignoring a possible halo component leads to a distortion of the spectrum in a small energy band, because of an incorrect background subtraction (depending on the distance from the source at which the background spectrum is taken); however, less soft photons would be "observed". A possibility is that we are including the halo in the extraction region. Since there is no obvious dust scattering model to fit the data, imaging may be the only way to test the halo hypothesis: given the particular modes adopted, this sort of analysis is very difficult (and altogether impossible in the burst mode). We only note that the dust scattering halo observed in Cyg X-2 (Costantini et al. 2005) has quite a broad spectrum (when normalized to the source spectrum), broader than the feature under discussion. Another problem with the scattering halo hypothesis is that the relative contribution of the excess is similar in the timing- and burst-mode observations, which is possible only if most of the halo is within 16", i.e. the width of the strip from which the timing-mode spectrum was extracted.

Even if unsatisfactory in many respects, the two above-mentioned hypotheses have the merit of invoking extended or off-axis emission, which can in principle help explain the presence of the excess in the pn spectra but not in the RGS. However, as the RGS spectrum is extracted over a region of about 2.5 arcminutes, the halo hypothesis seems to be excluded for the reasons discussed above. A confusing source, provided it lies at a greater distance, is instead still tenable. We note that all *Chandra* observations of GRS 1915+105 have been performed in the CC (i.e. non imaging) mode, therefore the above-mentioned hypotheses could not be tested yet.

In the assumption that the RGS spectrum suffers from instrumental/calibration problems, the 1 keV component could be related to the system, and a possible candidate would be the emission by a disk wind. Both a collisionally ionized plasma model and a photoionized plasma model do indeed fit the EPIC-pn data well.

In the first case, the temperature of the plasma is about 1.3 keV (obtained using the model), with metal abundance 1.2 times the solar value; the ISM absorber has an $N_{\rm H}$ of 9×10^{21} cm^{-2}. The emission integral is $7.2\times10^{57}d_{10}^2$ cm^{-3} (where d_{10} is the distance to the source in units of 10 kpc), which, assuming that the density of the matter is constant along the emitting region, translates into a mass of the wind $M_w \approx 6\ M_\odot d_{10}^2 n^{-1}$, where n is the number density. Assuming that the size of the disk wind is at most on the order of the binary separation (about 5×10^{10} cm according the binary system parameters given by Harlaftis & Greiner 2004), we obtain a lower limit to n of about $8\times10^{12}d_{10}$ cm^{-3}. With this size, the Thomson optical depth would already be substantial (~ 0.25), and be increasing further with decreasing size. Thus, the matter would not be really optically thin, so this solution is not self-consistent.

Alternatively, the matter may be in photoionization equilibrium with the emission due to reflection of the primary X–ray radiation. To model this case, we adopted a power law with the same photon index as the primary one (to model Thomson scattered radiation) plus a Gaussian line. In this case, the ISM $N_{\rm H}$ is larger, $\sim1.5\times10^{22}$ cm^{-2} (this value may be assumed as an estimate of the ISM column density)[10]. From the observed flux, the optical depth of the wind is about $0.001/f$, where f is the covering factor of the wind to the primary radiation. The centroid energy of the Gaussian line (~0.97 keV), its width (90 eV), and its EW against the reflected continuum (5.6 keV), all suggest a blend of Ne K and Fe L lines.

3.1.6. Other emission/absorption lines

Other emission and absoption lines are required to fit the spectrum. They are: two unresolved emission lines at about 1.85 keV and 2.25 keV, with EW=19 eV and 8 eV, respectively; two broad absorption lines at about 2.5 and 2.93 keV, with σ of 0.11 and 0.14 keV and EWs of −17 and −30 eV, respectively.

Some of these features may be instrumental artifacts, since this energy range is notoriously troublesome due to the changes

[10] For the sake of simplicity we fitted the absorption with a pure gas photoelectric absorption (model in XSPEC). Using a more appropriate ISM model that includes the effects of dust (TB in XSPEC, Wilms et al. 2000) does not change the results significantly. The fit returns basically the same χ^2 and the same column density.

in the effective area.[11] However, some of them appear too prominent to be entirely due to calibration problems. The first emission line can be readily identified with the Si recombination line. If arising from the same photoionized material responsible for the ∼1 keV excess (see above), its total EW would be about 16 keV, a very large but not fully unrealistic value, given the large overabundance we found in the local absorber and provided that the reflecting matter is still optically thin to resonant scattering (Matt et al. 1996), which is possible if the matter is largely turbulent. The same is true for the second emission line, which can be identified with Si and S , even if the best fit value of the energy is slightly lower.

More difficult to explain are the two broad absorption lines. The energies correspond to the Kα and Kβ recombination lines from S . In this case, the absorbing material cannot be the same as that responsible for the Fe absorption line (see Sect. 3.1.4), since the latter is more ionized. It is also worth recalling that the modeling of the absorption edges is oversimplified, because it does not take into account X-ray absorption fine structures (XAFS), which are generated if the material is in grains (e.g. Lee et al. 2002); this may introduce spurious features in the residuals, even if it cannot fully explain them. Moreover, we again stress that it is not inconceivable that a significant part of these features are of instrumental origin. Data with higher energy resolution and optimized calibration are necessary to solve this issue.

3.2. The burst-mode observation

We fitted the burst-mode spectrum with the same model used for the timing-mode spectrum, fixing those parameters that are not expected to vary. In particular, we fixed the interstellar absorption column density, the ratio between the elemental abundancies of the local absorber, and the iron abundance of the reflection component at the best fit values obtained for the timing-mode observation. A good fit (χ^2/d.o.f.=248.2/219) is found. The best fit parameters are summarized in Table 2.

In comparison with the timing-mode observation (see Fig. 7), the spectrum is steeper (Γ ∼2 instead of ∼1.7), and the reflection component much stronger (R ∼ 1.7 instead of 0.3) and more ionized (ξ ∼ 3300 instead of 940 erg cm s^{-1}). The inner and outer radii are much smaller (r_i <20, r_o ∼100). The local absorber is slightly larger, while the ionized iron disk lines are not detected (upper limits to the EW of about 10 eV for both the He– and H–like lines. The Fe H–like absorption line is still present, with a centroid energy of 6.98±0.02, i.e. consistent with both the rest frame value and the value obtained in the timing-mode observation. The EW is larger, about −50 eV, due to the fact that the line is now best fitted with a resolved width σ of 0.11±0.03 keV. The 1.85 and 2.24 keV emission lines are not required, with upper limits to the EWs of 5 and 2 eV, respectively. A 6.4 keV iron emission line is instead marginally found, with an EW of 6±4 eV.

[11] See Figs.30 and 31 in the XMM-*Newton* User's Handbook: http://xmm.vilspa.esa.es/external/xmm_user_support/documentation/uhb/node32.html .

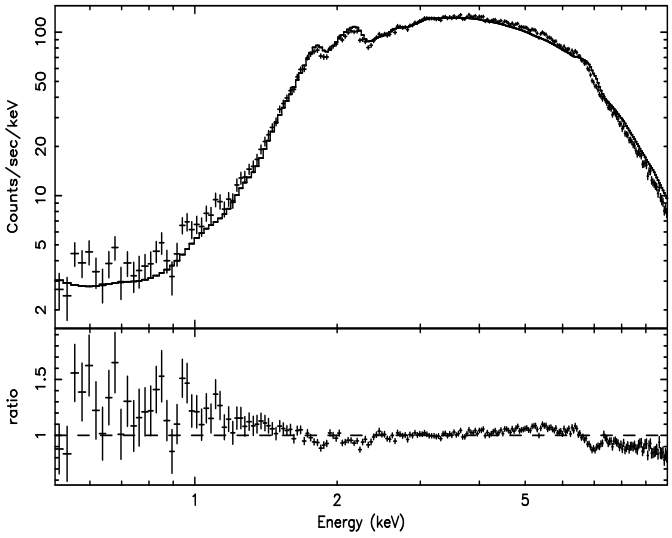

Fig. 7. The spectrum and data/model ratio of the burst-mode observation with the best fit model for the timing-mode observation. Clearly, iron line emission is over-subtracted, and the deficit at higher energies turns out to be more important than in OBS1; note again the strong excess at ∼ 1 keV and the wiggles at ∼ 2–3 keV (cp. with Fig. 5).

The above-mentioned results are consistent with a picture in which the disk is now more extended downwards and ionized (in fact, so ionized that no significant relativistic iron line is observed). The steeper spectrum can be due to the more efficient cooling, itself due to the increase in soft disk photons. The fact that no thermal disk emission is required, however, implies that the values for the inner and outer radii must be used with caution. It must be noted that they are now determined only via the reflection component, with all the associated uncertainties (see discussion in the previous section), as no disk line is present.

However, these results, especially those regarding the reflection components, can at least partly be an artifact due to calibration problems. A deficit of photons above 6÷7 keV, i.e. similar to what we find (see Fig. 7), is indeed also present in the burst-mode observation of the Crab Nebula (Kirsch et al. 2005), a source where of course no significant reflection component is expected.

The 1 keV excess, which still persists, can again be well fitted by a power law plus an emission line, the latter with a flux slightly larger than that obtained in the timing-mode observation. In the reflection scenario discussed in the previous section, the optical depth is about a factor 10 larger, which implies a much lower EW of the line. These findings can be explained, at least qualitatively, by assuming that the matter is now thicker to the lines, with consequent self-absorption effects (see e.g. Matt et al. 1996).

4. Conclusions

In this paper for the first time we have presented XMM-*Newton* observations of GRS 1915+105. Several problems make it difficult to observe the source fruitfully with this satellite, first of all due to the extremely high flux – in our case: $F_{2-10\ \mathrm{keV}}$ ∼

$6.0 \div 6.6$ (unabsorbed: $\sim 8.7 \div 10.7$) $\times 10^{-9}$ erg cm^{-2} s^{-1} – and to the notorious, erratic source variability, which does not help in triggering observations. We succedeed at both a) observing the source in a well-defined, stable physical/spectral state and b) collecting EPIC-pn useful data, only marginally corrupted by telemetry problems.

In both observations (April 17th and 21st, 2004), the source has been caught in a "plateau" state, also characterized by stronger jet activity and higher radio level, which we identify with the conventional "C" state / χ variability mode as defined by Belloni et al. (1997a,b, 2000). In this state the source shows a QPO at $\sim$ 0.6 Hz, i.e. what is expected in plateau intervals when the frequency vs. spectral hardness correlation is taken into account.

In order to try to disentagle the different spectral components, and thus to better discriminate among the viable spectral/physical models, we used the *rms* vs. E method by Ponti et al. (2004). The resulting *rms* is lower than 0.1 across the energy band. We further analyzed the variable $F_{\rm var}$, which takes the Poisson noise into account, and concluded that this variable is compatible with being null on the whole energy band, i.e. all spectral components are compatible with being constant during the two observations.

A priori, some of the features in the spectrum may be affected by dust halo scattering, although this cannot explain the 1 keV excess (see Sect. 3.1.5). However, testing this hypothesis would first of all require an accurate analysis based on proper source imaging (if available); further, spectral modelling of such effects is not easy (see e.g. Costantini et al. 2005). Being beyond the scope of this paper, this study should be addressed in future works.

We adopted a power law continuum model. This could be related to emission by a hot corona or to Comptonized thermal emission e.g. from the jet basis (as proposed by Rodriguez et al., 2004); however, an optically thick reflector is required to account for the smeared edge at $\sim$ 7 keV (with a covering ratio of $\sim 0.4 \div 1.7 \times 2\pi$ in the two observations, respectively). This may be evidence of an accretion disk being present, or just optically thick, only at quite a large distance from the central compact object, at least in the first observation ($r_i/r_g > 300$ in OBS1, $\sim$ 20 in OBS2). The relatively large amount of the reflection components implies that the primary X–ray emitting region should have a size that is at least comparable to the inner disk radius. That the disk is truncated, i.e. not present in the innermost part, is also suggested by the non-detection of a thermal disk emission component.

Several line residuals are superimposed on the modeled continuum. Part of these may be due to calibration uncertainties, especially at the energies where changes in the EPIC effective area take place (e.g. 1–3 keV). However, we found clear evidence of ionized iron emission around $\sim$ 7 keV: data are well fitted with two ionized Fe Kα lines, possibly affected by mild relativistic broadening (being produced far away from the BH event horizon), plus a narrow absorption feature at $\sim$ 6.95 keV.

The puzzling presence of an intense, broad excess around 1 keV can be explained in terms of reflection by an optically thin wind, provided that the feature is real and that the discrepancies between the RGS and pn spectra (discussed in Sections 2.2.1 and 3.1.5) have to be attributed to RGS calibration problems. This assumption is still unsubstantied, and should be regarded as a mere working hypothesis. The excess is indeed well fitted with a power law plus a line, unobscured by material that is intrinsic to the system. The centroid energy of the Gaussian line ($\sim$0.97 keV), its width (90 eV), and its EW against the reflected continuum (5.6 keV), together point to a blend of Ne K and Fe L lines. The value of the equivalent H column density is interestingly similar to the value of the obscuration by low Z elements (H, He, C, N, O) at the source core – $N_{\rm H} \sim 1.6 \times 10^{22}$ cm^{-2}: in the disk wind hypothesis, this may therefore be taken as an upper limit to the *interstellar* matter column density. This value matches the expected galactic absorption in that direction well (Dickey & Lockman 1990).

On the other hand, a significant fraction of the absorber must be *local* to the source. We adopted a variable absorption model (in XSPEC), assuming neutral matter and grouping the elements on the basis of both physical and practical considerations: elements which have probably a common origin, but also elements which are not very abundant (and therefore cannot be easily measured independently one from the other) with very abundant ones (e.g. Co and Ni with Fe): see the results in Table 1. A significant overabundance of the heavier elements compared to the lighter ones is apparent, which suggests that a significant fraction of the absorber, traced by heavier species, is local to the source. These results are somewhat different from those derived from *Chandra* HETG data (Lee et al. 2002): in particular, Fe and S abundances are roughly the same, while our values for Mg are about twice, and 2/3 for Si. The overall scenario is, however, very similar.

Clearly, the intrinsic absorption may be subject to substantial changes on longer timescales, as already observed with *Rossi*-XTE in similar plateaux (class χ, state C): from a mean value of $\sim 4.5 \times 10^{22}$ cm^{-2}, the total $N_{\rm H}$ may occasionally rise up to $\sim 6 \times 10^{22}$ cm^{-2} (Belloni et al. 2000).

Assuming the customary value of $\sim$ 12.5 kpc for the source's distance (Rodriguez & Mirabel, 1999) we obtain an estimate of the intrinsic luminosity $L^{\rm unabs}_{2-10\ {\rm keV}} = 1.7 \div 2.0 \times 10^{38}$ erg s^{-1} in the two observations.[12]

5. Acknowledgments

The authors would like to thank Stefano Bianchi, Laurence Boirin, Massimo Cappi, Michal Dovčiak, Ken Ebisawa, Yaël Fuchs, Matteo Guainazzi, Mariano Mendez, Markus Kirsch, Jon Miller, Christian Motch, the anonymous referee, and the whole XMM-*Newton* Helpdesk staff at Vilspa for many useful suggestions and technical help. Radio data at 15 GHz were observed with the Ryle Telescope, Cambridge, and kindly supplied by Guy Pooley. *Rossi*-XTE ASM (All Sky Monitor) results were provided by the teams at MIT and at the RXTE SOF and GOF at NASA's GSFC. AM wishes to thank the French Space Agency CNES, the University Paul Sabatier in Toulouse,

[12] Some authors claim that the distance could be substantially smaller (by up to a factor $\sim 1/2$: see Chapuis & Corbel 2004), in which case a corresponding correction of the luminosity (and BH mass) estimate should be considered.

and the CNRS Research Group "Phénomènes Cosmiques de Haute Energie" for financial support, as well as the Astronomical Institute of the Czech Academy of Sciences for their very kind hospitality. TB acknowledges partial support by grants INAF-PRIN 2002 and MIUR-PRIN 2003027534_004. VK acknowledges the grant ref. GAAV IAA 300030510. GP thanks the European Commission under the Marie Curie Early Stage Research Training program for support.

References

Anders, E., & Grevesse, N. 1989, Geochim. et Cosm. Acta 53, 197
Belloni, T., Mendez, M., King, A.R., van der Klis, M., & van Paradijs, J. 1997a, ApJ 479, L145
Belloni, T., Mendez, M., King, A.R., van der Klis, M., & van Paradijs, J. 1997b, ApJ 488, L109
Belloni, T., Klein-Wolt, M., Mendez, M., van der Klis, M., & van Paradijs, J. 2000, A&A 355, 271
Belloni, T., Homan, J., Casella, P., van der Klis, M., Nespoli, E., Lewin, W.H.G., Miller, J.M., Mendez, M. 2005, A&A, in press
Bianchi, S., Matt G., Nicastro F., Porquet D., Dubau J., 2005, MNRAS, 357, 599
Boirin, L., Mendez, M., Diaz Trigo, M., Parmar, A.N., Kaastra, J.S. 2005, A&A 436, 195
Castro-Tirado, A.J., Brandt, S., & Lund, N. 1992, IAU Circular n.5590
Chapuis, C., & Corbel, S. 2004, A&A 414, 659
Costantini, E., Freyberg, M.J. & Predhel, P. 2005, A&A – in press: astro-ph/0508129
Dickey, J.M., & Lockman, F.J. 1990, ARA&A 28, 215
Done, C., Wardzinski, G., Gierlinski, M. 2004, MNRAS 349, 393
Ehle, M., Breitfellner, M., González Riestra, R., Guainazzi, M., et al. 2004, "XMM-*Newton* Users' Handbook" Issue 2.2, online edition – http://xmm.vilspa.esa.es/external/xmm_user_support/documentation/uhb/index.html
Fender, R.P., et al. 1999, MNRAS 304, 865
Fender, R., & Belloni, T. 2004, ARA&A 42, 317
Feroci, M., Costa, E., Matt, G., Belloni, T., Tavani, M. 1998, Nucl. Phys. B (Proc. Suppl.) 69/1-3, 336
Foster, R.S., Waltman, E.B., Tavani, M., Harmon, B.A., Zhang, S.N., Paciesas, W.S., Ghigo, F.D. 1996, ApJ 467, L81
Fuchs, Y., Rodriguez, J., Mirabel, I.F. et al. 2003, A&A 409, L35
Greiner, J., Morgan, E.H., & Remillard, R.A. 1998, New Astr. Rev. 42, 597
Greiner, J., et al. 2001, A&A 373, L37
Greiner, J., Cuby, J.G., & McCaughrean, M.J., 2001, Nature 414, 522 (2001b)
Hannikainen, D.C., Vilhu, O., Rodriguez, J., et al. 2003, A&A 411, L415
Hannikainen, D.C., et al. 2004, in: Proc. of the 5th *INTEGRAL* Workshop, Munich 16-20 February 2004. Published by EDP – in press: astro-ph/0405349
Hannikainen, D.C., Rodriguez, J., Vilhu, O., et al. 2005, A&A 435, 995
Harlaftis, E.T., & Greiner, J. 2004, A&A 414, L13
Homan, J., & Belloni, T. 2005, in: Proc. of the Workshop "From X-ray Binaries to Quasars: Black Hole Accretion on All Mass Scales", Eds. T.J. Maccarone, R.P. Fender, L.C. Ho (Dordrecht: Kluwer), in press – in press: astro-ph/0412597
Kirsch, M. 2005, "EPIC Status of Calibration and Data Analysis", XMM-SOC-CAL-TN-0018 – http://xmm.vilspa.esa.es/external/xmm_sw_cal/calib/documentation/index.shtml#EPIC
Kirsch, M., et al. 2005, "Crab: the standard X-ray candle with all (modern) X-ray satellites" – astro-ph/0508235
Lee, J.C., et al. 2002, ApJ 567, 1102
Maccarone, T.J., 2002, MNRAS 336, 1371
Martocchia, A., Matt, G., Karas, V., Belloni, T., Feroci, M. 2002, A&A 387, 215
Martocchia, A., Matt, G., Karas, V., Belloni, T., Feroci, M. 2004, in: Proc. II *Beppo*SAX Symposium, *The restless high-energy universe*, Amsterdam (The Netherlands), 5-8/5/2003. Eds. E.P.J. Van den Heuvel, J.J.M. In't Zand and R.A.M.J. Wijers, Elsevier, Nucl. Physics B (Proc. Suppl.) 132, 404
Matt, G., Brandt, W.N, Fabian, A.C. 1996, MNRAS, 280, 823
Miller, J.M., Fabian, A.C., Nowak, M.A., Lewin, W.H.G., 2004, in: Proc. 10th Annual Marcel Grossmann Meeting on General Relativity, in press – astro-ph/0402101
Mirabel, I.F., & Rodriguez, L.F. 1994, Nature 371, 46
Muno, M., Remillard, R., Morgan, E. et al. 2001, ApJ 556, 515
Ponti, G., Cappi, M., Dadina, M., Malaguti, G. 2004, A&A 417, 451
Pooley, G., & Fender, R., 1997, MNRAS 292, 925
Reig, P., Belloni, T., van der Klis, M. (2003), A&A 412, 229
Rodriguez, L.F., & Mirabel, I.F. 1999, ApJ 511, 398
Rodriguez, J., Corbel, S., Hannikainen, D.C., Belloni, T., Paizis, A., Vilhu, O. 2004, ApJ 615, 416
Trudolyubov, S.P. 2001, ApJ 558, 276
Wilms, J., Allen, A., McCray, R. 2000, ApJ 542, 914

	Power law
Γ	$1.686^{+0.008}_{-0.012}$
	Cold absorption
$N_{\rm H,He,C,N,O}$	$1.60^{+0.17}_{-0.29} \times 10^{22}$ cm^{-2}
$N_{\rm Ne,Na}$	$7.46^{+0.31}_{-0.72} \times 10^{22}$ cm^{-2}
$N_{\rm Mg,Al}$	$7.57^{+0.54}_{-0.16} \times 10^{22}$ cm^{-2}
$N_{\rm Si}$	$5.70^{+0.07}_{-0.12} \times 10^{22}$ cm^{-2}
$N_{\rm S}$	$4.69^{+0.07}_{-0.69} \times 10^{22}$ cm^{-2}
$N_{\rm Cl,Ar,Ca,Cr}$	$11.0^{+1.3}_{-1.6} \times 10^{22}$ cm^{-2}
$N_{\rm Fe,Co,Ni}$	$11.7^{+0.2}_{-0.2} \times 10^{22}$ cm^{-2}
	Emis. lines
E_l	$1.846^{+0.006}_{-0.005}$ keV
F_l	$1.35^{+0.15}_{-0.07} \times 10^{-2}$ ph cm^{-2} s^{-1}
EW	19 eV
E_l	$2.244^{+0.007}_{-0.010}$ keV
F_l	$3.62^{+0.46}_{-0.62} \times 10^{-3}$ ph cm^{-2} s^{-1}
EW	8 eV
	Abs. line
E_l	$6.95^{+0.01}_{-0.03}$ keV
F_l	$-7.9^{+0.2}_{-0.1} \times 10^{-4}$ ph cm^{-2} s^{-1}
EW	-9 eV
σ	1 eV (frozen)
	1st disk line (He-like Fe)
E_c	6.7 keV (fixed)
r_i/r_g	580^{+210}_{-120}
F_l	$2.37^{+0.18}_{-0.18} \times 10^{-3}$ ph cm^{-2} s^{-1}
EW	28 eV
	2nd disk line (H-like Fe)
E_c	6.96 keV (fixed)
r_i/r_g	320^{+80}_{-60}
F_l	$2.20^{+0.19}_{-0.21} \times 10^{-3}$ ph cm^{-2} s^{-1}
EW	28 eV
	Reflection
$R/2\pi$	$0.35^{+0.02}_{-0.02}$
$A_{\rm Fe}$	$5.2^{+0.7}_{-1.9}$
ξ	940^{+190}_{-80} erg cm s^{-1}
r_i/r_g	320^{+80}_{-60}
$F_{2-10\ \rm keV}$	~ 0.6 (unabs: ~ 0.87) 10^{-8} erg cm^{-2} s^{-1}
χ^2/d.o.f.	317.5/227

Table 1. The best fit model parameters for the timing-mode observations. The column densities are the Hydrogen equivalent column for solar abundances as in Anders & Grevesse (1989). The outer radii of the reflection and disk line models have been linked together in the fit, yielding $r_o/r_g = 900^{+190}_{-90}$; r_i in the 2nd disk line model has been linked together to r_i of the reflection component. See the text for further discussion.

	Power law
Γ	$2.04^{+0.01}_{-0.02}$
	Cold absorption
$N_{\rm H,He,C,N,O}$	$1.98^{+0.02}_{-0.02} \times 10^{22}$ cm^{-2}
	Reflection
$R/2\pi$	$1.69^{+0.16}_{-0.04}$
r_i/r_g	<20
r_o/r_g	93^{+11}_{-17}
ξ	3300^{+600}_{-600} erg cm s^{-1}
$F_{2-10\ \rm keV}$	~ 6.6 (unabs: ~ 10.7) 10^{-9} erg cm^{-2} s^{-1}
χ^2/d.o.f.	248.2/219

Table 2. The best fit model parameters for the burst-mode observation (OBS2). See the text (Sect. 3.2) for details.